

Changes in Extreme Precipitation Accumulations during the Warm Season over Continental China

MEIYU CHANG,^a BO LIU,^a CRISTIAN MARTINEZ-VILLALOBOS,^{b,c} GUOYU REN,^{a,d} SHANGFENG LI,^e AND TIANJUN ZHOU^f

^a Department of Atmospheric Science, School of Environmental Studies, China University of Geosciences, Wuhan, China

^b Department of Atmospheric and Oceanic Sciences, University of California, Los Angeles, Los Angeles, California

^c Centro de Estudios Avanzados en Zonas Áridas, Coquimbo, Chile

^d Laboratory for Climate Studies, National Climate Center, China Meteorological Administration, Beijing, China

^e Jilin Provincial Key Laboratory of Changbai Mountain Meteorology and Climate Change, Laboratory of Research for Middle-High Latitude Circulation Systems and East Asian Monsoon, Institute of Meteorological Sciences of Jilin Province, Changchun, China

^f LASG, Institute of Atmospheric Physics, Chinese Academy of Science, Beijing, China

(Manuscript received 4 August 2020, in final form 14 September 2020)

ABSTRACT: Precipitation accumulations, integrated over rainfall events, are investigated using hourly data across continental China during the warm season (May–October) from 1980 to 2015. Physically, the probability of precipitation accumulations drops slowly with event size up to an approximately exponential cutoff scale s_L where probability drops much faster. Hence s_L can be used as an indicator of high accumulation percentiles (i.e., extreme precipitation accumulations). Overall, the climatology of s_L over continental China is about 54 mm. In terms of cutoff changes, the current warming stage (1980–2015) is divided into two periods, 1980–97 and 1998–2015. We find that the cutoff in 1998–2015 increases about 5.6% compared with that of 1980–97, with an average station increase of 4.7%. Regionally, s_L increases are observed over East China ($10.9\% \pm 1.5\%$), Northwest China ($9.7\% \pm 2.5\%$), South China ($9.4\% \pm 1.4\%$), southern Southwest China ($5.6\% \pm 1.2\%$), and Central China ($5.3\% \pm 1.0\%$), with decreases over North China ($-10.3\% \pm 1.3\%$), Northeast China ($-4.9\% \pm 1.5\%$), and northern Southwest China ($-3.9\% \pm 1.8\%$). The conditional risk ratios for five subregions with increased cutoff s_L are all greater than 1.0, indicating an increased risk of large precipitation accumulations in the most recent period. For high precipitation accumulations larger than the 99th percentile of accumulation s_{99} , the risk of extreme precipitation over these regions can increase above 20% except for South China. These increases of extreme accumulations can be largely explained by the extended duration of extreme accumulation events, especially for “extremely extreme” precipitation greater than s_{99} .

KEYWORDS: Atmosphere; Asia; Extreme events; Precipitation; Trends

1. Introduction

Precipitation extremes are generally projected to increase on continental to global scales (Sun et al. 2007; Kharin et al. 2013; Pendergrass and Hartmann 2014; Donat et al. 2016), as has been observed during recent decades (Westra et al. 2013; Donat et al. 2016), implying greater risks of flooding (IPCC 2014). A large body of literature focuses on the change of extreme precipitation (Donat et al. 2016; Trenberth 2011; Sillmann et al. 2013; Zhai et al. 2005; Ma et al. 2015; Ma and Zhou 2015; Di et al. 2015; P. Yang et al. 2017; Shi et al. 2015; Xu et al. 2018; Wasko and Nathan 2019; Zhang and Zhou 2019), often by applying a high percentile that is taken as the threshold of extreme precipitation (e.g., the 95th percentile) of the cumulative frequency distribution of daily precipitation. However, varying percentiles used by different studies may lead to different conclusions when considering the responses of extreme precipitation to global warming (Pendergrass 2018).

Therefore, it is necessary for researchers to carefully choose a physically motivated definition of extreme precipitation.

In this study we employ the cutoff scale of the probability distribution of precipitation accumulations as an indicator of extreme precipitation (Neelin et al. 2017). Precipitation accumulation is defined as the total amount of precipitation during the course of a precipitation event (from event onset to termination), representing the integrated moisture loss during an event. The shape of probability distribution of precipitation accumulations has been documented in several studies (García-Marín et al. 2007; Peters et al. 2001, 2010; Deluca and Corral 2010, 2014; Martínez-Villalobos and Neelin 2019) and consists of an approximate power-law range with the probability density gradually decreasing with an increase of accumulation size up to a certain cutoff scale s_L and then dropping sharply after it (Neelin et al. 2017). This implies that this cutoff scale controls the extreme tail of the probability distribution. Indeed, Martínez-Villalobos and Neelin (2018, hereafter MN18) use the cutoff scale to study the changes in precipitation accumulation extremes over the United States and show that there is a significant positive correlation between s_L and high accumulation percentiles, further validating the application of the cutoff scale as the threshold of extreme precipitation.

Furthermore, Stechmann and Neelin (2011, 2014) establish a theoretical model for the distribution of precipitation event

Supplemental information related to this paper is available at the Journals Online website: <https://doi.org/10.1175/JCLI-D-20-0616.s1>.

Corresponding author: Bo Liu, boliu@cug.edu.cn

DOI: 10.1175/JCLI-D-20-0616.1

© 2020 American Meteorological Society. For information regarding reuse of this content and general copyright information, consult the AMS Copyright Policy (www.ametsoc.org/PUBSReuseLicenses).

sizes and give a definition of the precipitation accumulation cutoff scale s_L . According to these studies, the cutoff scale s_L is controlled by the interplay between the integrated moisture loss and moisture convergence variance; thus, as moisture convergence fluctuations are expected to increase in most regions under current global warming, the cutoff scale also increases. Specifically, the accumulation cutoff scale combines in one scale the effects of event duration as well as thermodynamic (due to changes in moisture) and dynamic (due to changes in circulation) effects on extremes (Martinez-Villalobos and Neelin 2019). On the other hand, compared to the cutoff scale precipitation percentiles are artificially selected values and are more sensitive to resolution and to the left-censoring of precipitation time series (MN18).

Using observational and reanalysis datasets, previous studies have analyzed changes of extreme precipitation in past decades over China. Overall, increasing trends were found for all of China, but this trend exhibited distinct regional features (Xu et al. 2011; Zhai et al. 2005; Wang and Zhou 2005; Liu et al. 2005; You et al. 2011; Ma and Zhou 2015; Ma et al. 2017; Zhou et al. 2016). For example, based on the daily precipitation data over China during the period 1961–2001, Wang and Zhou (2005) showed that extreme daily precipitation events increased significantly in Northwest China whereas it decreased significantly in North China and Northeast China. Using high-resolution gridding data (CN05) over China during the period 1961–2010, Zhou et al. (2016) found that total amount of precipitation from extremely wet days (R95p) demonstrated positive trends in Northwest China, South China, and East China and negative trends in Northeast China and North China. These studies mainly focused on daily precipitation with the application of extreme indices, especially the high percentiles of the cumulative frequency distributions. Ma et al. (2015) analyzed the frequency of occurrence of daily precipitation, but mainly focused on the changes in precipitation amount and frequency of different decades. Until now, however, there have been no studies investigating precipitation accumulation distributions and their changes based on rain gauge data over China. We note that Eastern China is one of the regions with the largest expected increase in accumulation extremes by the end of the century (Neelin et al. 2017), which provides further motivation to document trends in accumulation extremes in current climate.

In this study, we analyze the climatological and recent changes of the precipitation accumulation cutoff scale. Unlike previous research on daily precipitation extremes, the accumulation framework allows us to partition changes in extremes between trends in event duration (from precipitation onset and termination) and intensity. According to the observational hourly precipitation data during the warm season (May–October) from 1980 to 2015, we calculate cutoff scales over continental China and its subregions in the context of global warming. Moreover, we also compare these results derived from precipitation accumulation with those derived from daily precipitation. We show evidence that the cutoff scales of the probability distributions of precipitation accumulations and daily precipitations are useful indicators in depicting precipitation

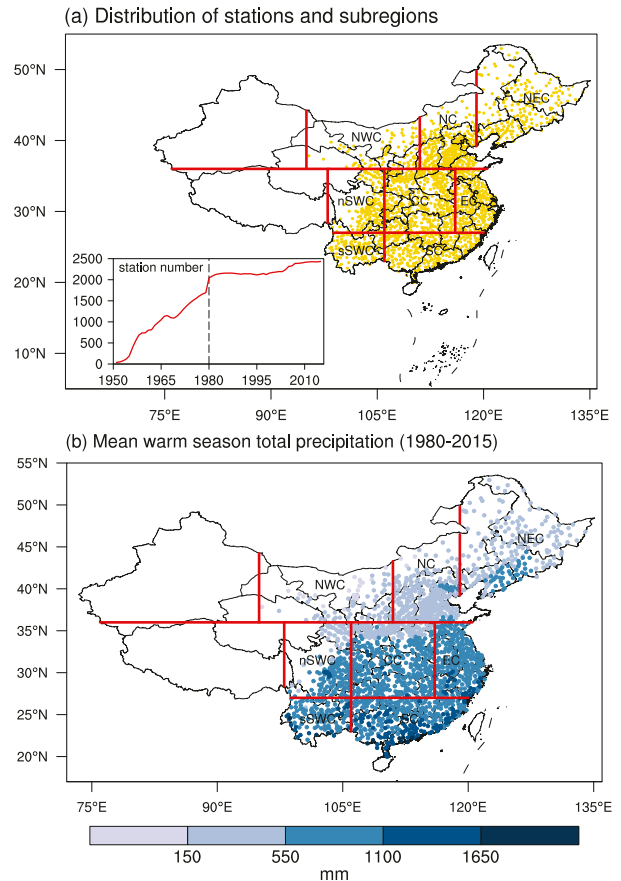


FIG. 1. (a) Locations of the 1910 rain gauge stations used in this study. (b) Multiyear (1980–2015) mean of total precipitation during the warm season (May–October). The color box of the legend in (b) represents the range within the adjacent two labels. Red lines denote eight subregions of China: Northeast China (NEC), North China (NC), Northwest China (NWC), East China (EC), Central China (CC), northern Southwest China (nSWC), southern Southwest China (sSWC), and South China (SC). Evolution of number of stations over China during the warm season between 1951–2015 is shown in the small inset in (a).

extremes and exhibit an overall increase in extreme precipitation accumulations over continental China.

2. Data and methods

a. Hourly precipitation data

In this study, we use observational hourly precipitation data at 1910 stations over China (Fig. 1a) obtained from the National Meteorological Information Centre (NMIC) of the China Meteorological Administration (CMA), covering the period of 1980–2015 during the warm season (May–October), to investigate the probability distributions of precipitation accumulations. The warm season includes late spring, summer (June–August) and early autumn, in which the precipitation accounts for more than 80% of the annual total for most of the observational stations (Ren et al. 2015). The period of 1980–2015

is used because the hourly precipitation data are available for the high-density observational network (Fig. 1a, inset), and also it is an abnormally rapid climate warming stage of the last century in China and East Asia (Ren et al. 2017).

To examine the regional features of accumulation distributions and their changes, these stations are grouped into eight different climate regions based on China's National Assessment Report on Climate Change (National Report Committee 2007): Northeast China (NEC), North China (NC), Northwest China (NWC), East China (EC), Central China (CC), Qinghai-Tibet Plateau (SWC1), Southwest China (SWC2), and South China (SC). Due to the uneven station density, we have excluded the western parts of NWC and SWC1 and renamed SWC1 and SWC2 as northern Southwest China (nSWC) and southern Southwest China (sSWC), respectively (Fig. 1a). The distribution of mean total precipitation amount during the warm season (May–October) is shown in Fig. 1b, there is an increase moving toward the southeast: the low values are located over NEC, NC, and NWC and the high values are located over EC, CC, SC, nSWC, and sSWC.

Note that the geographical pattern of stations follows the geographical pattern of population (Ren et al. 2010), which leaves the western part of the country undersampled. This implies that aggregated results in NWC and SWC (nSWC and sSWC) regions reflect mainly the eastern part of these regions. Meanwhile, when we aggregate the precipitation data of all stations to calculate probability density function (PDF) in China, the all-China results mainly reflect the eastern part of the country.

b. Calculation of cutoff scale

As described in MN18, the precipitation accumulation s is defined as the total accumulated precipitation from the exceedance of a small threshold (0.1 mm h^{-1} is used in this study as it is the resolution of precipitation data) to the drop below the threshold, and the formula, for continuous data, is given by

$$s = \int_{t_i}^{t_f} R(t) dt, \quad (1)$$

where $R(t)$ is the precipitation intensity (mm h^{-1}) at time t , with t_i and t_f the start time and the end time of the precipitation event, respectively. For hourly precipitation data (as in this study), the integral in (1) is replaced by a summation. Previous studies (Peters et al. 2010; Deluca and Corral 2014; Stechmann and Neelin 2014) have shown that the PDF of precipitation accumulations p_s is

$$p_s \propto s^{-\tau} \exp(-s/s_L), \quad (2)$$

with τ being the exponent of the power-law range (usually >1) and s_L the cutoff scale. Similarly, to compare the PDF of precipitation accumulations with that of daily precipitation P , we fit daily precipitation PDFs (p_P) using a gamma distribution (Groisman et al. 1999; Cho et al. 2004) of the form

$$p_P \propto P^{-\tau_P} \exp(-P/P_L). \quad (3)$$

Typically, $\tau > 1$ while $\tau_P < 1$, which is the main difference for both distributions and is illustrated in Figs. 2c and 2d.

There are several ways these parameters could be estimated (e.g., Peters et al. 2010; Deluca and Corral 2014). One simple way to estimate τ and s_L can be found in appendix A of Martinez-Villalobos and Neelin (2019). Here, we just provide a review. By taking the logarithm of (2), a relationship between functions of s and $\log(p_s)$ is as follows:

$$\log(p_s) = c_1 + c_2 \log(s) + c_3 s, \quad (4)$$

where c_1 is a constant and $c_2 = -\tau$, $c_3 = -(1/s_L)$. Then we can estimate the c_i coefficients by a simple multivariate linear regression and the parameters are given as $\tau = -c_2$ and $s_L = -(1/c_3)$. The daily precipitation PDF parameters τ_P and P_L in (3) can be estimated by using the same method. The PDFs of precipitation accumulation and daily precipitation over continental China during the warm season for the period of 1980–2015 are shown in Figs. 2a and 2b. As can be seen, the probability density gradually decreases with the increase of accumulation size s or daily precipitation P , and drops rapidly after the cutoff scale. The effect of the cutoff scale s_L (or P_L) in controlling the probability of largest precipitation events is obvious compared to the probability distributions without cutoff scales as illustrated by the dashed lines (Figs. 2a,b). Moreover, the difference of the power-law part between accumulations and daily precipitation is also apparent (Figs. 2c,d), with accumulations falling faster within the power-law range (Fig. 2a).

It should be noted that for this method the fit of the accumulation PDF is a prerequisite for the method in (4), and the derivations of s_L (P_L) and τ (τ_P) have a slight dependence on the binning scheme, making it complicated to use s_L (P_L) to investigate precipitation. According to previous studies (Peters et al. 2010; Stechmann and Neelin 2014; Muschinski and Katz 2013; MN18), s_L is approximately proportional to the moment ratio s_M . And hence here we estimate the cutoff scale s_L using moment ratio s_M , which is defined as the ratio of the second moment to the mean moment of s and the formula is given by

$$s_M = \frac{\langle s^2 \rangle}{\langle s \rangle}. \quad (5)$$

Similarly, for daily precipitation P (over wet days, $P \geq 0.1 \text{ mm}$), the moment ratio P_M is defined as

$$P_M = \frac{\langle P^2 \rangle}{\langle P \rangle}. \quad (6)$$

3. Results

a. Climatology of precipitation accumulation cutoff scale

Consistent with MN18, significant positive correlation ($r = 0.95$) is found over China between s_M and accumulation 99th percentile s_{99} at each station for the period of 1980–2015 (Fig. 3a). Meanwhile, significant positive correlations (statistically significant at the 1% level; not shown in the paper) are also found between s_M and other high percentiles (s_{90} , s_{95} , s_{97} , $s_{99.9}$), indicating that the cutoff can be used as a predictor of the behavior of extreme accumulation percentiles. Moreover, similar high positive correlations exist between P_M and P_{99}

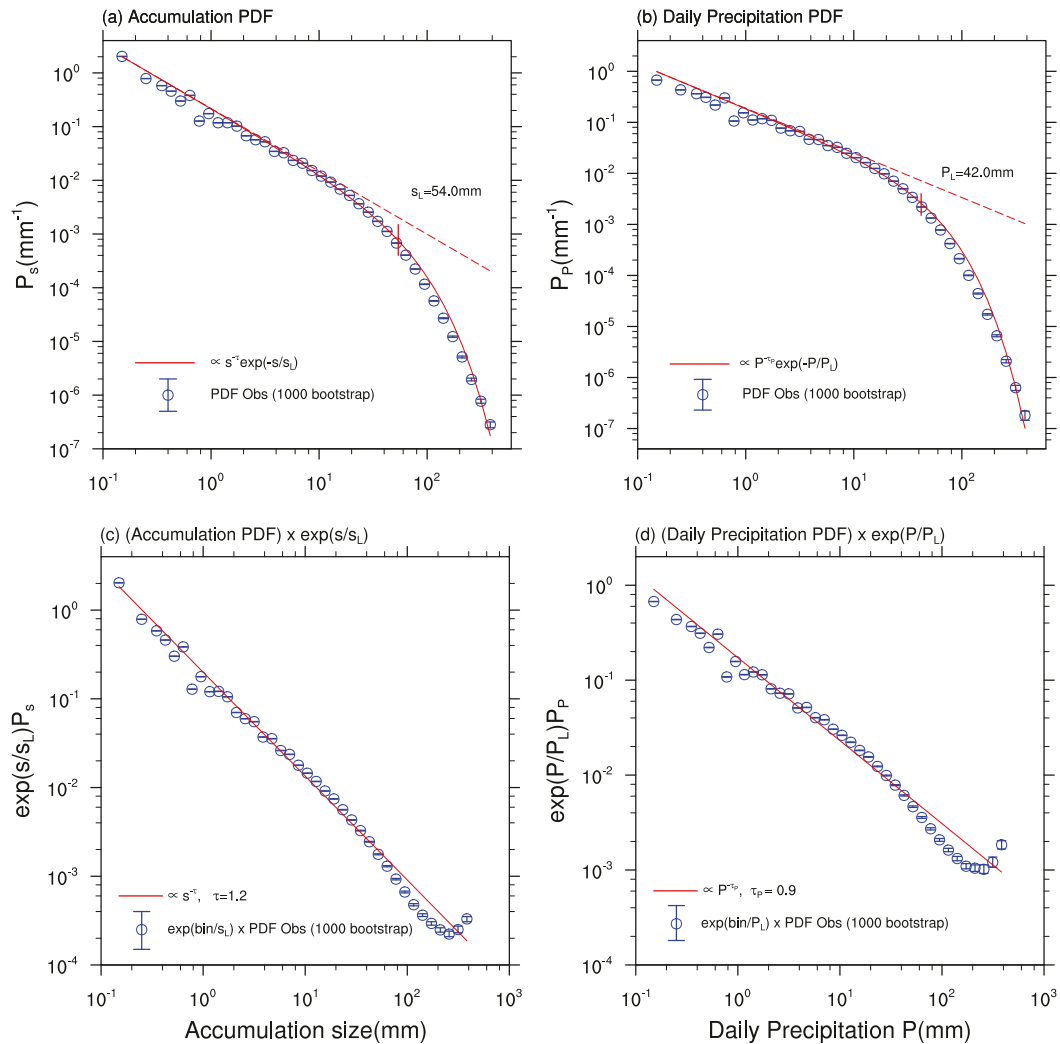


FIG. 2. (a) Accumulation PDF and (b) daily precipitation PDF over China during 1980–2015 period. (c),(d) The power-law part of accumulation precipitation and daily precipitation distributions, respectively. The error bars indicate the results from 1000 bootstrap (with replacement) realizations (5th–95th), and the circles represent the median value. The solid red lines in (a) and (b) represent the fitting lines given by (2) and (3), respectively. The red dashed lines in (a) and (b) solely represent the power-law part of (2) and (3), respectively.

($r = 0.97$) (Fig. 3b) as well as between s_M and P_M ($r = 0.98$) (Fig. 3c). Therefore, we can safely infer that the conclusions derived from precipitation accumulations hold true for daily precipitation.

Figure 4 gives the climatological distribution of s_M for each station (Fig. 4a) and eight regions (Fig. 4b) in 1980–2015, with high values mainly distributed over EC, CC, and SC and low values over NEC, NWC, and sSWC, resembling largely that of mean warm season total precipitation (Fig. 1b). Also, this spatial pattern resembles those of heavy precipitation days and very heavy precipitation days (Ma et al. 2015).

The cutoff is distinct from traditional percentile definitions of extreme precipitation in that it is a physically motivated scale, unlike percentiles, set by the balance between moisture loss due to precipitation and moisture convergence (Neelin

et al. 2017; Martinez-Villalobos and Neelin 2019). Physically, accumulations larger than s_L occur in a regime where moisture convergence outpaces moisture loss by precipitation, and opposite for accumulations smaller than s_L (Neelin et al. 2017). In other words, a uniform high percentile (e.g., 95th percentile) may correspond to precipitation occurring in different dynamical regimes. Figure 5 displays the nearest precipitation percentile (with a resolution of 0.1) to the climatological s_L for each station (Fig. 5a) and each region (Fig. 5b). Obviously, the nearest percentile to the climatological s_L for each station and region is different. For example, the threshold of extreme accumulations is $s_{98.9}$ in nSWC while in NWC this threshold is s_{97} (Fig. 5b). Even in the same region, for instance nSWC, the precipitation percentiles corresponded to the s_L , ranging from less than s_{91} to greater than s_{98} (Fig. 5a).

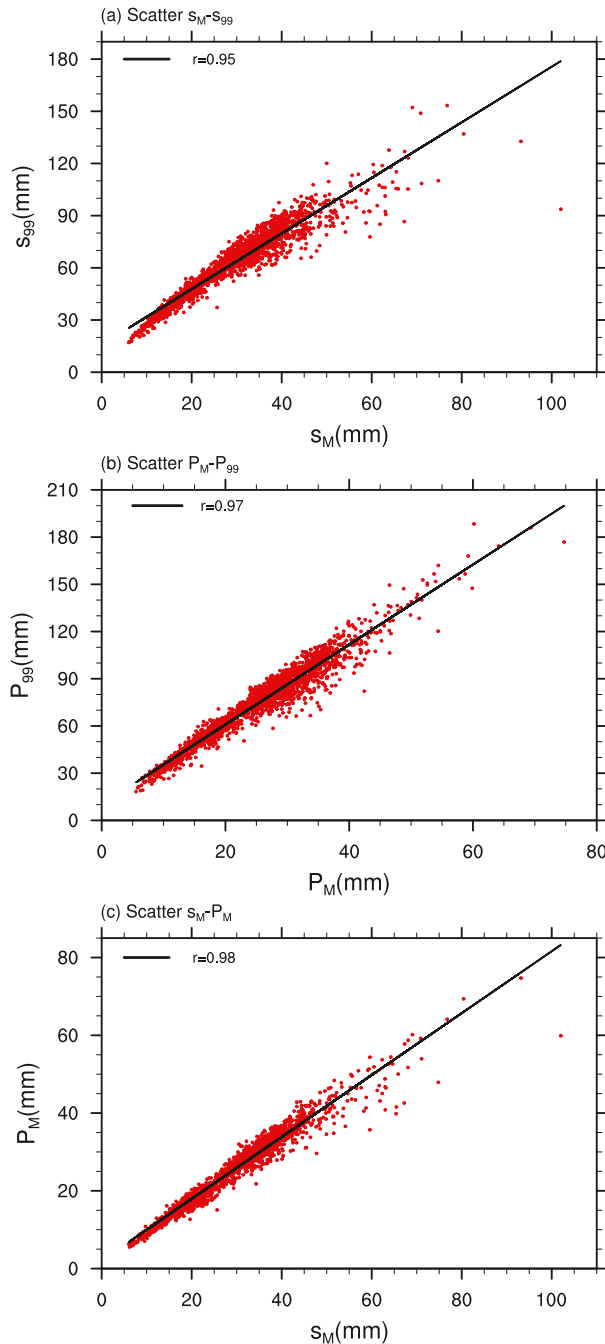


FIG. 3. (a) The scatter of s_M and precipitation accumulation 99th percentile s_{99} at each station. (b) The scatter of P_M and P_{99} at each station. (c) The scatter of s_M and P_M at each station.

b. Changes of cutoff scale for eight subregions

To investigate the changes of precipitation accumulations in a warming climate, here we divided the whole period into two equal periods, 1980–97 and 1998–2015. We have calculated percentage changes of s_M at each station (Fig. 6a). The formula for calculating the percentage change is given by

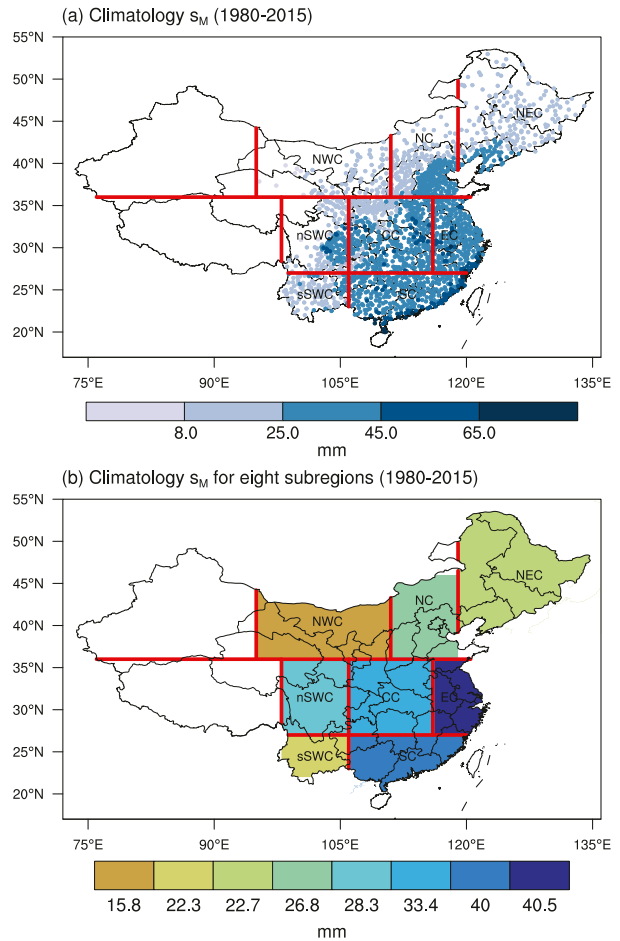


FIG. 4. (a) The spatial distribution of s_M at each station during 1980–2015 period. (b) The climatological distribution of s_M for eight divisions. The color box of the legend in (a) represents the range within the adjacent two labels while the color box of the legend in (b) represents the label at the center of the color box.

percentage change

$$= [(s_M|_{1998-2015} - s_M|_{1980-97})/s_M|_{1980-97}] \times 100\%. \quad (7)$$

Overall, compared to the former period (1980–97), the number of stations with increased s_M accounts for about 58.5% of the total during the recent period (1998–2015), with an average increase of 4.7% in s_M across stations.

In general, s_M (~34.1 mm) during 1998–2015 increased about 5.6% compared with that (~32.3 mm) of 1980–97 over continental China. Figure 6b shows the mean percentage changes of s_M for eight divisions, based on 1000 bootstrap (with replacement) realizations. Regionally, increases of s_M are found over five out of eight regions—EC (10.9% ± 1.5%; mean ± standard errors), NWC (9.7% ± 2.5%), SC (9.4% ± 1.4%), sSWC (5.6% ± 1.2%), and CC (5.3% ± 1.0%) (Fig. 6c)—indicating that extreme precipitation accumulations increased during past three or four decades over these regions. Decreases of s_M are found over three regions: NC (−10.3% ± 1.3%),

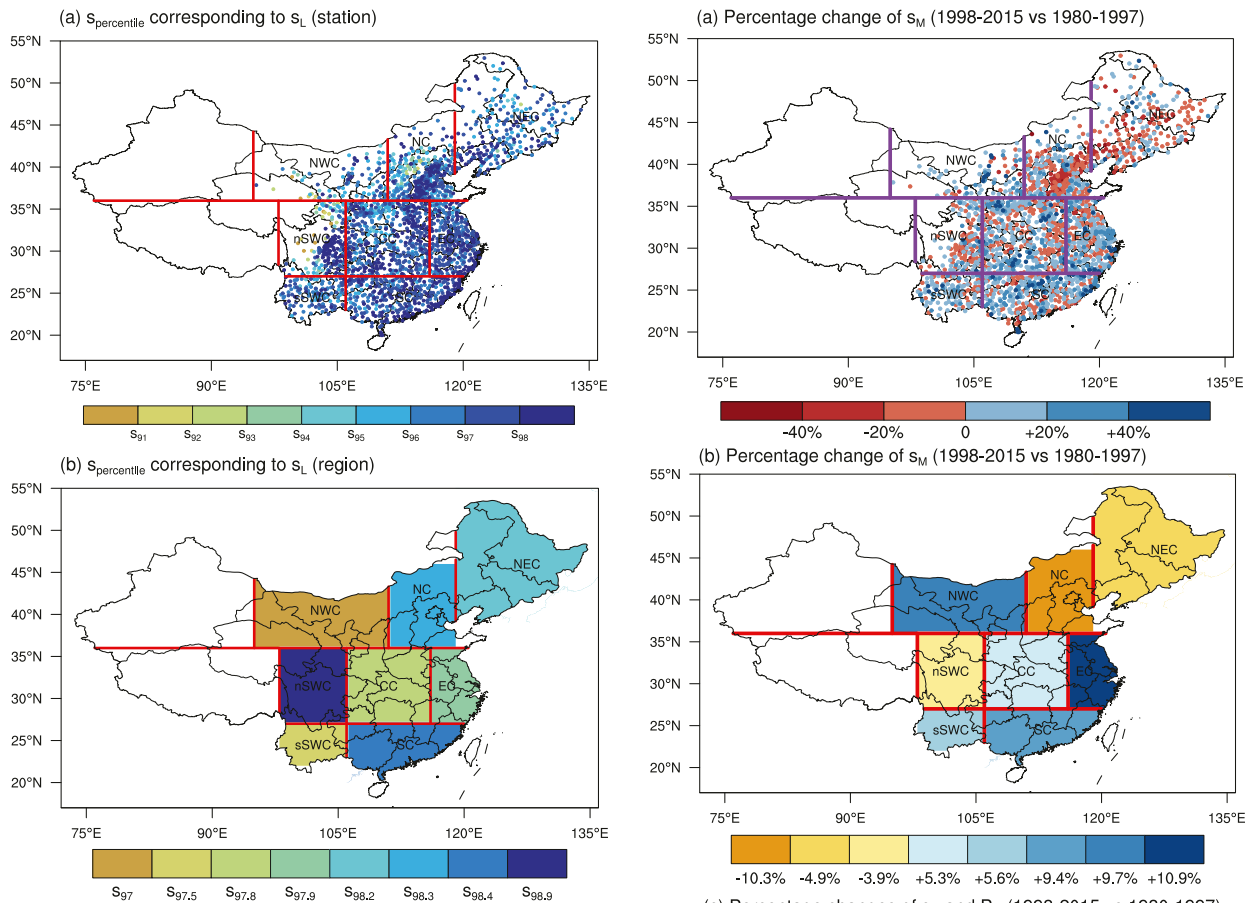


FIG. 5. The nearest percentile of the climatologically s_L for (a) each station and (b) each region. The reference percentiles are from the 90th to 99.9th percentile with an interval of 0.1. Note that the color box of the legend in (a) represents the range within the adjacent two labels while the color box of the legend in (b) represents the label at the center of the color box.

NEC ($-4.9\% \pm 1.5\%$), and nSWC ($-3.9\% \pm 1.8\%$) (Fig. 6c). The behaviors of P_M between the two periods resemble those of s_M for all subregions (Fig. 6c), implying that precipitation accumulation is also highly correlated with daily precipitation when it comes to the changes. Note that changes in P_M are smaller in amplitude than those of s_M , consistent with MN18. Furthermore, changes in P_M are largely consistent with trends in daily extreme precipitation indices during the last decades reported in previous studies (Zhou et al. 2016; Ma et al. 2015; P. Yang et al. 2017). For instance, Zhou et al. (2016) revealed similar decreasing trends in R95p over North China and Northeast China, in accordance with the decreasing trend of P_M . In addition, the spatial patterns of changes in s_M and P_M resemble those of changes in mean daily precipitation for the warm season (Fig. S1 in the online supplemental material), indicating that the change of extreme precipitation revealed by cutoff is related to the changes of mean precipitation. This spatial pattern of decadal changes in precipitation is closely related to natural factors (Zhang 2015) such as thermal forcing

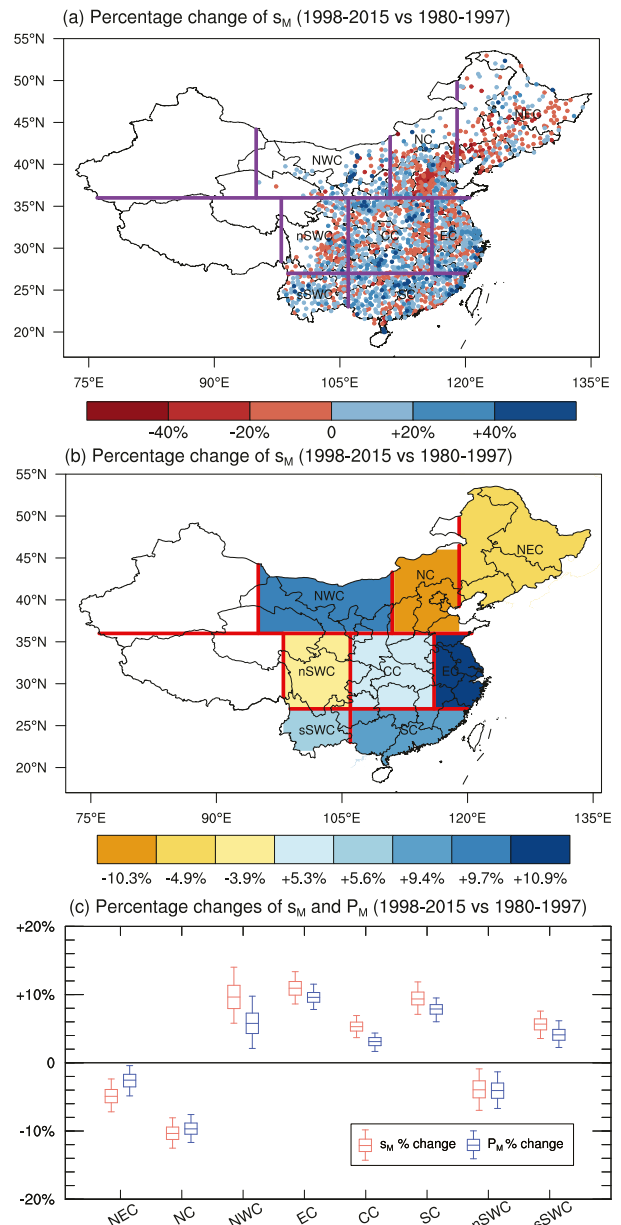


FIG. 6. (a) Percentage change of s_M at each station and (b) mean percentage change of s_M for each climate division between 1998–2015 and 1980–97 (1998–2015 minus 1980–97). (c) Percentage changes of s_M and P_M for eight climate divisions between 1980–97 and 1998–2015. The results in (b) and (c) are based on 1000 bootstrap (with replacement) realizations, and the boxes in (c) represent the 50th percentile with the error bars represent the 5th–95th percentiles. The color box of the legend in (a) represents the range within the adjacent two labels while the color box of the legend in (b) represents the label at the center of the color box.

over the Tibetan Plateau (Duan et al. 2013) and Pacific decadal oscillation (e.g., Q. Yang et al. 2017).

To examine the changes of the PDF associated with the changes of s_L , we calculated the PDFs for the three regions (NWC, EC, and SC; Fig. 6c), with the biggest s_M (or P_M)

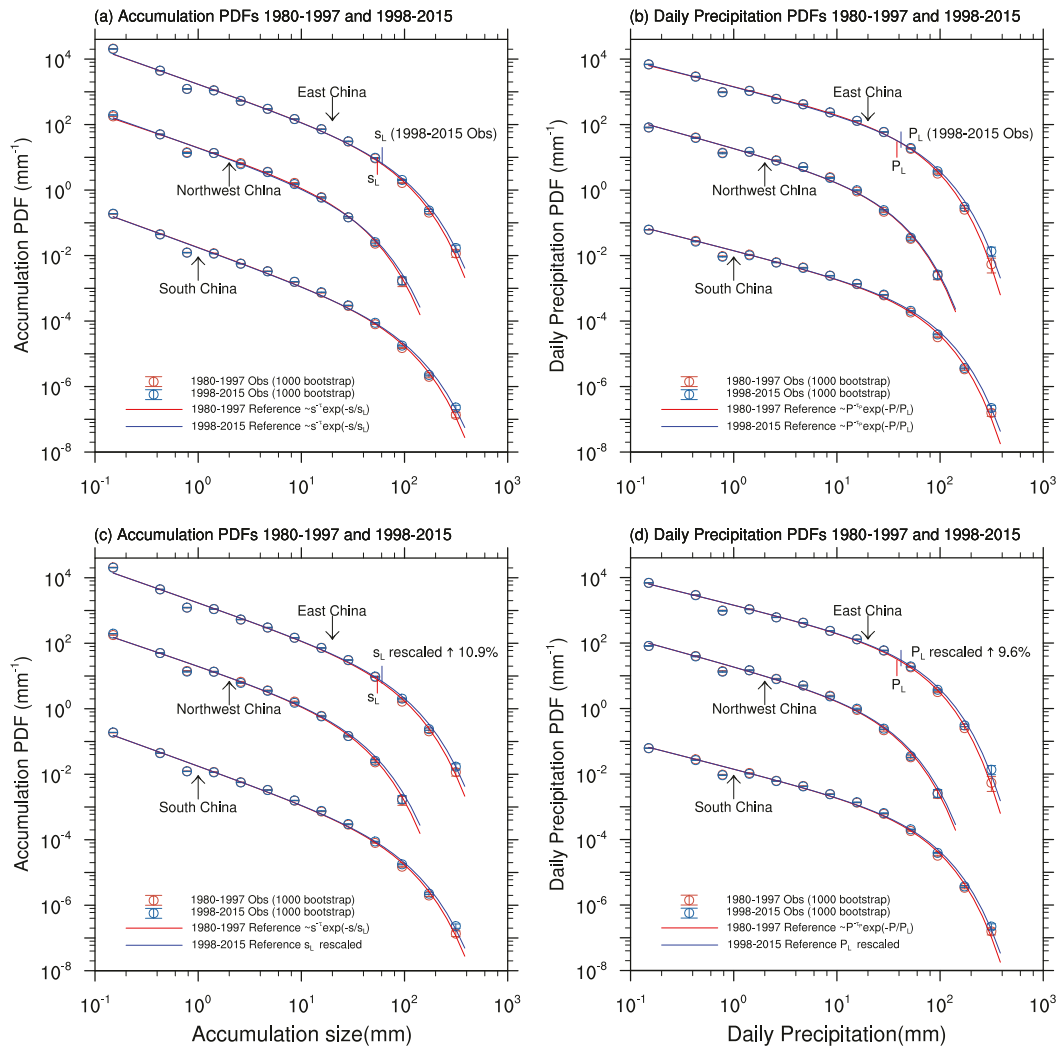


FIG. 7. The PDFs of (a) accumulation and (b) daily precipitation calculated over the 1980–97 (red) and 1998–2015 (blue) for the EC, NWC, and SC regions with biggest s_M increases (East China PDFs $\times 10^4$, Northwest China PDFs $\times 10^2$, South China PDFs $\times 10^{-1}$). The error bars indicate the results from 1000 bootstrap (with replacement) realizations (5th–95th), and the circles represent the median value. The red lines in (a) and (b) are fitted by $As^{-\tau} \exp(-s/s_L)$ [or $BP^{-\tau} \exp(-P/P_L)$] and superimposed on the 1980–97 accumulations (daily precipitation) observed PDFs, and the blue lines in (a) and (b) are fitted by the same formula and superimposed on the 1998–2015 accumulations (daily precipitation) observed PDFs. (c),(d) As in (a) and (b), but s_L (or P_L) of 1998–2015 is replaced by the rescaled version through increasing the percentage change of mean s_M (or P_M) over these regions (Fig. 6b).

increases between the two periods (Fig. 7). As can be seen, the relative changes of PDFs in two periods are obvious in the extreme tails for accumulation and daily precipitation, implying a larger fraction of extreme precipitation events in 1998–2015 (Figs. 7a,b). These increases in extreme precipitation events are associated with the increases in s_L (or P_L), which are well represented in the distributions of 1998–2015 by just rescaling s_L (Figs. 7c,d). The above analysis demonstrated that the cutoff scale s_L is physically linked to the shape of probability distribution of precipitation accumulations. That is, the changes of s_L can be regarded as an indicator of changes of the full extreme tails of PDFs.

Moreover, to further compare with the results using different high percentiles, here the percentage changes of s_M (or P_M) and different percentiles (90th, 95th, 97th, 99th, 99.9th) for accumulation and daily precipitation are shown in Fig. 8. For accumulations, it can be seen that the changes of different percentiles are nearly consistent in the sign except for NWC and nSWC regions, but the amplitudes differ (Fig. 8a). In NWC, s_{95} shows a negative trend but s_{99} has a positive trend. A similar situation is also revealed in the changes of the different percentiles for daily precipitation (Fig. 8b). It is worth noting that the changes in lower percentiles (e.g., the 90th and 95th percentiles, which may be located in the power-law range of

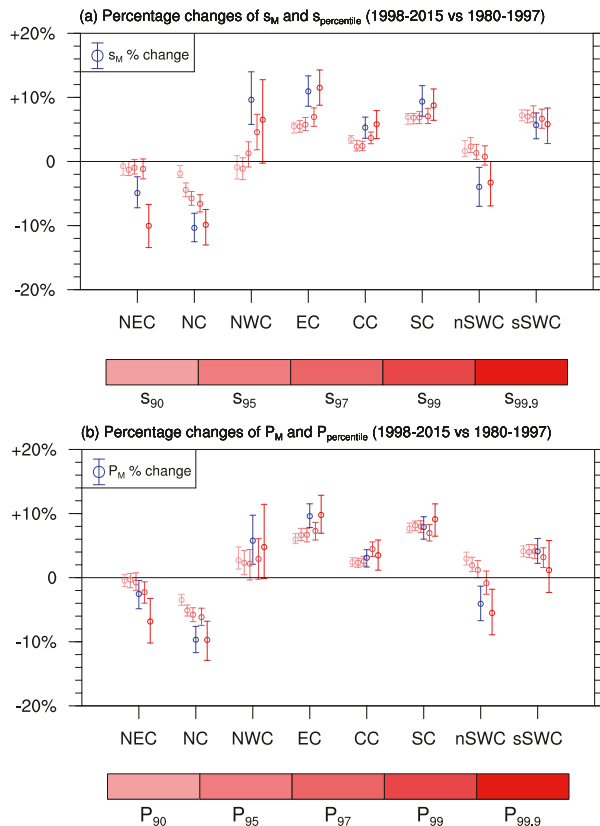


FIG. 8. (a) Percentage changes of s_M and different percentiles ($s_{90}, s_{95}, s_{97}, s_{99}, s_{99.9}$) of accumulation precipitation for eight climate divisions between 1980–97 and 1998–2015. (b) Percentage changes of P_M and different percentiles ($P_{90}, P_{95}, P_{97}, P_{99}, P_{99.9}$) of daily precipitation for eight climate divisions between 1980–97 and 1998–2015. The results in (a) and (b) are based on 1000 bootstrap (with replacement) realizations, and the boxes represent the 50th percentile with the error bars represent the 5th–95th percentiles.

the PDF) of NWC and nSWC are unclear, but the behaviors of higher percentiles tend to follow those of s_M or P_M . These results show that using different precipitation percentiles may lead to conflicting conclusions regarding changes in extreme precipitation, consistent with Pendergrass (2018). Meanwhile, the changes of percentiles above the percentile corresponding to s_L (P_L) are well predicted by the changes in the respective cutoff scales.

c. Ratio of accumulation probability density

For large precipitation events, the changes of the PDFs are consistent with the changes of cutoff scales (Figs. 7a,b), meaning that large precipitation event risks may increase. Hence we calculate the conditional risk ratios between the two periods to illustrate this. We define a risk ratio as

$$r_s(\hat{s}) = \frac{\int_{\hat{s}}^{\infty} p_s'' ds'}{\int_{\hat{s}}^{\infty} p_s' ds'} \quad (8)$$

which represents the ratio of probability of accumulations larger than \hat{s} between 1998–2015 (p_s'') and 1980–97 (p_s'). Here p_s'' and p_s' are the probability densities calculated from the accumulation precipitation larger than \hat{s} in 1998–2015 and 1980–97, respectively. The risk ratios can give information of changes related to precipitating processes, because they only depend on changes of the precipitating regime dynamics for accumulations (MN18).

Based on the percentage change of s_M , we have calculated the risk ratios for the regions with increased s_M (Fig. 9). We label the position of the x axis with different accumulation percentiles to understand the changes of probability for accumulations. When the five regions with increased s_M are regarded as a whole, the risk ratio has an increasing trend and exceeds 1.2 for the accumulation size greater than $s_{99.9}$, meaning that the risk of extreme accumulation increases as the cutoff scale is extended. Consistently, the conditional risk ratios for five subregions with increased cutoff s_M are all greater than 1.0 and gradually increase, also implying an increased risk of large precipitation accumulations, which may be further accentuated under global warming (Neelin et al. 2017; Norris et al. 2019). As can be seen, the probability of accumulations is nearly identical for small accumulations, while for large accumulations, significant changes are indicated by the risk ratios. Taking into account sampling variability, the shape of the risk ratios is roughly consistent with theoretical expectations (e.g., Martinez-Villalobos and Neelin 2019, their Fig. 8), observational estimates in the United States (MN18), and climate model projections (Neelin et al. 2017). For example, over CC, the risk ratio is slowly increasing with the accumulation size up to about s_{96} , and then followed by a rapid increase where the accumulation size exceeds approximately s_{99} . For accumulations larger than s_{99} , the risk ratios in these regions can reach above 1.2 except for SC. These results indicate that, with the extension of the cutoff scale in the PDF of precipitation accumulations, large accumulations exhibit significant increase in 1998–2015 compared to the former period. Similarly, the risk of extreme accumulation decreases for the three subregions with decreased s_M (Fig. S2). More importantly, the change of cutoff scale allows one to explain changes in the whole extreme tail of the PDF [see Fig. 8 in Martinez-Villalobos and Neelin (2019) for more details], while the change of an extreme percentile provides little information by itself about how the whole PDF is changing.

d. Changes of extreme accumulation: The role of event duration and event-mean intensity

Next, we move to resolve whether changes of the intensity or the duration should be responsible for changes in the PDF of precipitation accumulations.

An advantage of the accumulation framework is that we can attribute changes to changes in event duration and event intensity. To separate the effects of event duration (h) and event-mean intensity (mm h^{-1}) on extreme accumulation, we have calculated the changes in the number of events, mean duration, mean intensity (averaged over event), and size of accumulation extremes (mean accumulation of extreme accumulation events) (Fig. 10). Similar to MN18, we used a regional threshold ranging from s_M to

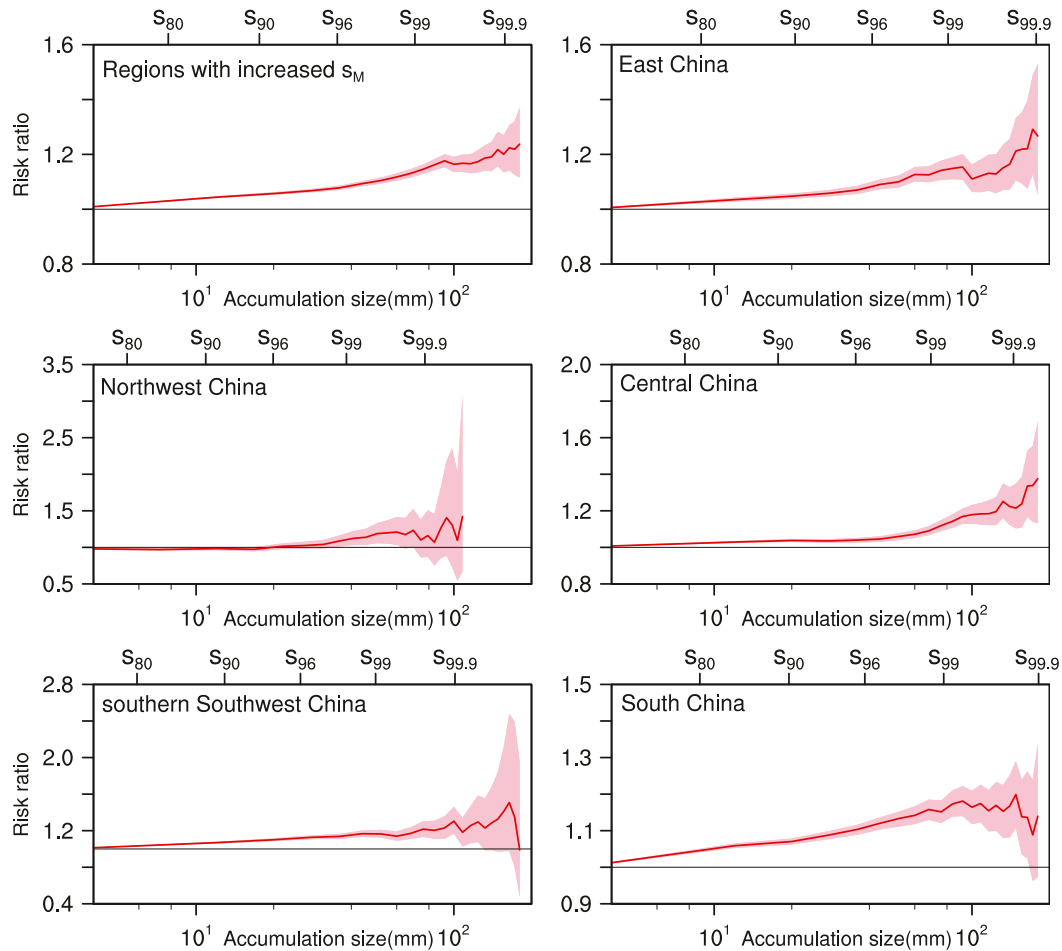


FIG. 9. Accumulation risk ratios (conditioned on event occurrence), calculated from (8), for the five regions with increased s_M . Note that the first one in the first row is obtained by taking the five regions with increased s_M as a whole. The solid red line represents the risk ratios from observations, and the pink shadow represents the 5th–95th percentiles based on 1000 bootstrap (with replacement) realizations. The top x axis is labeled with the position of different accumulation percentiles.

$5s_M$ (s_M is calculated using the whole period of 1980–2015) to select accumulation events and to investigate why extreme accumulations change over these regions. The range of s_M – $5s_M$ is used so that a variety of configurations with different balances between number of samples and how extreme the events are can be sampled. For example, s_M contains many samples of events starting in the moderate extreme range, whereas $5s_M$ contains fewer samples with only the most extreme events. Moreover, for the sake of comparison with results from the common definition of extreme precipitation, we also label the position of the x axis with several corresponding accumulation percentiles. As can be seen, s_M and $5s_M$ correspond to at least accumulation 97th and 99.9th percentiles, respectively, covering “moderate” to “extreme” extreme precipitation.

Overall, when taking the regions (EC, CC, SC, NWC, and sSWC) with extended cutoff as a whole (first row of Fig. 10), the number of extreme events and the size of accumulation extremes exhibit consistent positive trends. Moreover, for

accumulations larger than s_{99} , it can be clearly seen that positive trends of extreme accumulations result from the increased durations, rather than intensity (first row of Fig. 10). Similarly, the decrease of extreme accumulations is also mainly due to the decrease of duration (first row of Fig. S3). Regionally, similar trends in event number and size of accumulation extremes are also found for the five regions with increased s_M , except for sSWC where the change of accumulations is not significant (Fig. 10). Note that there are regional differences in the changes of duration and intensity. For NWC, which was reported to be wetting during past decades (Wang and Zhou 2005; Zhou et al. 2016; P. Yang et al. 2017), the extended duration and weakened intensity are consistently found across the selected range of extreme accumulations. Similar situations are also found for CC, where the very heavy precipitation events had increased (Ma et al. 2015). For EC, the strengthened intensity appeared in the “moderately” extreme accumulations approximately under s_{99} , but the positive duration plays an

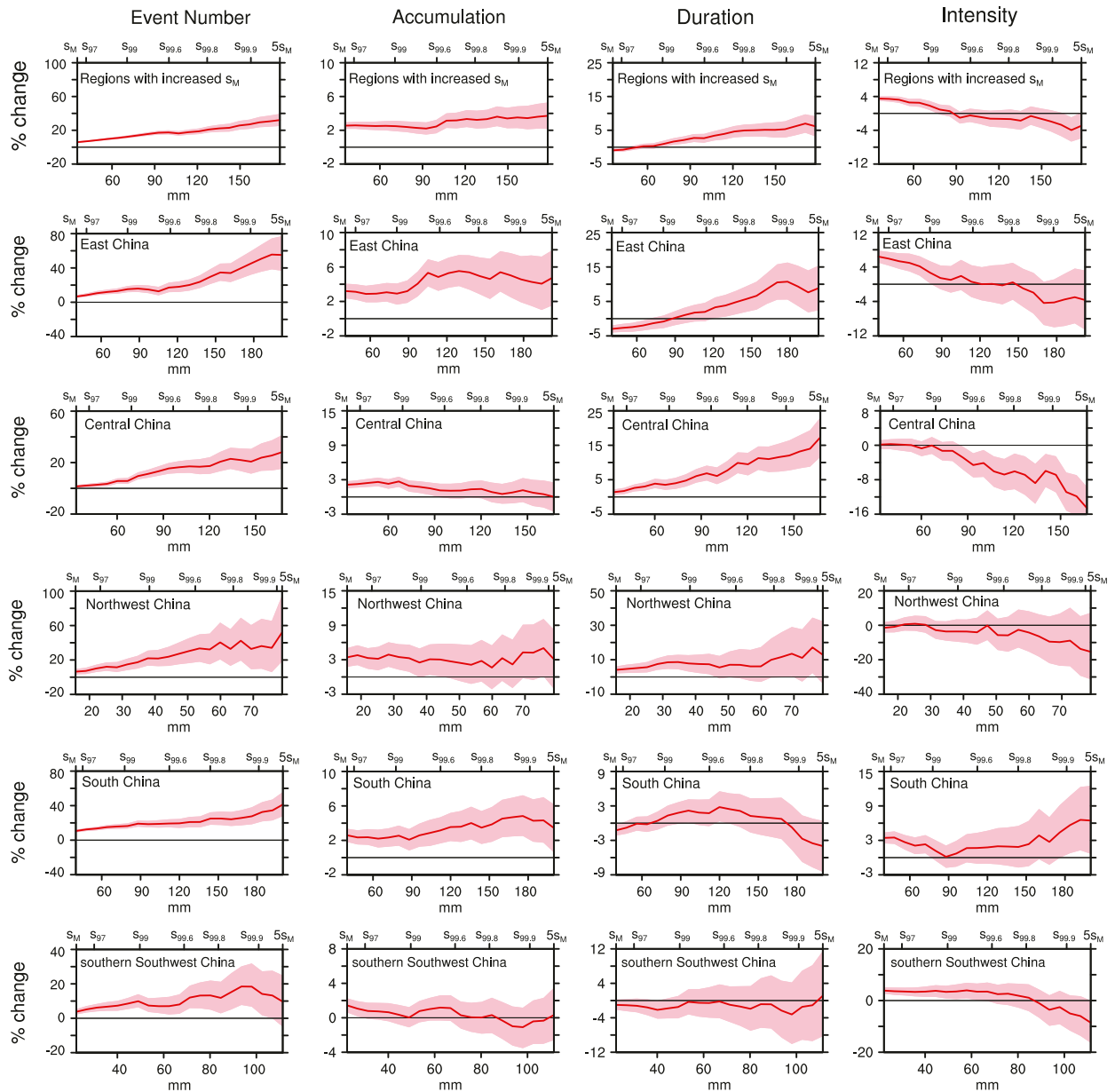


FIG. 10. Changes in (first column) the number of events, (second column) mean accumulation, (third column) mean event duration, and (fourth column) mean event intensity of extreme accumulation events larger than a regional threshold ranging from s_M to $5s_M$ between 1998–2015 and 1980–97 for five regions with increased s_M : (second row) East China, (third row) Central China, (fourth row) Northwest China, (fifth row) South China, and (sixth row) southern Southwest China. The first row is obtained by taking the five regions with increased s_M as a whole. It is worth noting that the left end of the x axis corresponds to s_M and the rightmost corresponds to $5s_M$. The value of s_M used here is calculated by using the whole period 1980–2015. The solid red line represents the changes from observations, and the pink shadow represents the 5th–95th percentiles based on 1000 bootstrap (with replacement) realizations. The top x axis is labeled by the position of different accumulation percentiles.

important role in the change of accumulation for extreme accumulations larger than s_{99} . However, for SC and sSWC, the strengthened intensity seems to better explain the change in accumulation, although the increase of duration and the decrease of intensity appeared in the middle intervals spanning from about 99th percentile to about 99.8th percentile

accumulations for SC. These regional results suggest that at least for “extremely” extreme precipitation larger than s_{99} , the positive trend is mostly from the elongated duration, which are in line with the results obtained by taking the regions with increased s_M as a whole (first row of Fig. 10). Furthermore, for three subregions with decreased s_M , the number of extreme

events and size of extreme accumulations show negative trends (Fig. S3). Indeed, negative trends of extreme accumulations also result from the shortened duration, rather than the reduced intensity (Fig. S3). In conclusion, the changes of extreme events and accumulations are largely consistent with the changes of cutoff scale and the changes of size of accumulation extremes are mostly affected by the mean duration. Note that changes in P_M resemble those of s_M , implying that the results derived from precipitation accumulations apply also to daily precipitation.

4. Summary and discussion

In this study, using hourly rain gauge measurements from 1910 stations, we investigated the climatology and recent changes of precipitation accumulation distributions over continental China during the warm season. Overall, the climatological cutoff s_L of precipitation accumulation distributions is about 54 mm over China. At the station level, we find the cutoff scale in each station to be positively correlated with extreme accumulation percentiles, indicating that the cutoff scale can be used to study extreme precipitation over China. Similar positive correlation occurs for daily precipitation. Moreover, the cutoff scales of precipitation accumulations and daily precipitation are highly correlated, implying that the results derived from precipitation accumulations can be used to explain extreme precipitation indices derived from daily precipitation data. On a regional scale, the distribution of cutoff s_L is roughly like that of mean warm season total precipitation, with the maximal values mainly located over East, Central, and South China.

We divided the whole period into two equal periods (1980–97 and 1998–2015) to investigate changes of precipitation accumulation in the context of current warming climate. In general, the number of stations with increased s_L accounts for about 58.5% of the total and the overall cutoff scale increases about 5.6% over continental China in 1998–2015. Overall, the regions with increased or decreased cutoff were characterized with similar increasing or decreasing trends in event number or size of accumulation extremes (Fig. 10 and Fig. S3). However, changes of cutoff s_L exhibit distinct regional features. On a regional scale, increases were found over East China ($10.9\% \pm 1.5\%$), Northwest China ($9.7\% \pm 2.5\%$), South China ($9.4\% \pm 1.4\%$), southern Southwest China ($5.6\% \pm 1.2\%$), and Central China ($5.3\% \pm 1.0\%$). Also, three out of eight subregions witnessed the decrease of cutoff scale, namely, North China ($-10.3\% \pm 1.3\%$), Northeast China ($-4.9\% \pm 1.5\%$), and northern Southwest China ($-3.9\% \pm 1.8\%$). Changes derived from daily precipitation resemble those of precipitation accumulations but with smaller magnitude. Furthermore, we found that the changes of the PDFs of accumulation and daily precipitation in the right tails can be well represented by rescaling the cutoff scales (Fig. 7), which can be used as a simple prototype for future changes in the extreme tail (Neelin et al. 2017; MN18).

For five subregions with increased cutoff, the conditional risk ratios are gradually increasing and all larger than 1.0, and especially for high accumulations larger than s_{99} , the risk ratios are larger than 1.2 over five regions except for South China,

suggesting that there are significant increases for large accumulations greater than s_{99} during 1998–2015 compared to the 1980–97 period. In addition, the number of extreme events and size of extreme accumulations for five regions with increased s_L have an overall increasing trend. The increased size of extreme accumulations can be largely accounted for by an extension of the mean duration of these extreme events, especially for “extremely extreme” precipitation greater than approximately s_{99} .

The dominating role of duration, rather than intensity, in explaining increases in accumulation is consistent with other observational estimates in the United States (MN18) and global warming climate model projections in midlatitudes (Norris et al. 2019). Since extreme accumulations are highly correlated to extreme daily precipitation, this framework highlights the different factors controlling daily versus hourly precipitation intensities (Lenderink and van Meijgaard 2008; Barbero et al. 2017; MN18). While hourly intensities are generally projected to increase (Lenderink and van Meijgaard 2008; Prein et al. 2017), the most extreme hourly precipitation may not be contributing to the most extreme daily precipitation, as the latter may be mainly controlled by increases in event duration.

The trends of extreme precipitation over China indicated by the changes of accumulation cutoffs over different regions are largely consistent with previously studies during the last decades (Xu et al. 2011; Liu et al. 2005; You et al. 2011; Zhou et al. 2016; Ma et al. 2015; P. Yang et al. 2017). Over continental China, the cutoff scales of the probability distributions of precipitation accumulations and daily precipitations are demonstrated to be useful in depicting precipitation extremes, and provide a complement to studies focusing on changes in extreme percentiles. This analysis and previous studies (Ren et al. 2015) showed a more obvious rise in extreme precipitation processes of shorter duration than those of longer duration in China over the last decades, and this might have also been related to other factors than global climate warming such as urbanization effect, aerosols effect and possibly the systematic bias induced by weakening wind speed (Rosenfeld et al. 2008; Ren et al. 2016; Zheng and Ren 2017). All of these factors combine to produce increases in the cutoff scale in most of the regions studied. The good prediction of the changes in extreme tails of PDFs by rescaling the cutoff (Fig. 7) provides a useful prototype to understand future changes of precipitation extremes.

Acknowledgments. This work was supported by the National Key R&D Program of China (2018YFA0605604).

REFERENCES

- Barbero, R., H. J. Fowler, G. Lenderink, and S. Blenkinsop, 2017: Is the intensification of precipitation extremes with global warming better detected at hourly than daily resolutions? *Geophys. Res. Lett.*, **44**, 974–983, <https://doi.org/10.1002/2016GL071917>.
- Cho, H., K. P. Bowman, and G. R. North, 2004: A comparison of gamma and lognormal distributions for characterizing satellite rain rates from the Tropical Rainfall Measuring Mission. *J. Appl. Meteor.*, **43**, 1586–1597, <https://doi.org/10.1175/JAM2165.1>.
- Deluca, A., and Á. Corral, 2010: Power laws and scaling of rain events and dry spells in the Catalonia region. Preprints, Centre

- de Recerca Matemàtica, 22 pp., <http://hdl.handle.net/2072/152168>.
- , and —, 2014: Scale invariant events and dry spells for medium-resolution local rain data. *Nonlinear Processes Geophys.*, **21**, 555–567, <https://doi.org/10.5194/npg-21-555-2014>.
- Di, T., Y. Guo, and W. J. Dong, 2015: Future changes and uncertainties in temperature and precipitation over China based on CMIP5 models. *Adv. Atmos. Sci.*, **32**, 487–496, <https://doi.org/10.1007/s00376-014-4102-7>.
- Donat, M. G., A. L. Lowry, L. V. Alexander, P. A. O’Gorman, and N. Maher, 2016: More extreme precipitation in the world’s dry and wet regions. *Nat. Climate Change*, **6**, 508–513, <https://doi.org/10.1038/nclimate2941>.
- Duan, A., M. Wang, Y. Lei, and Y. Cui, 2013: Trends in summer rainfall over China associated with the Tibetan Plateau sensible heat source during 1980–2008. *J. Climate*, **26**, 261–275, <https://doi.org/10.1175/JCLI-D-11-00669.1>.
- García-Marín, A. P., F. J. Jiménez-Hornero, and J. L. Ayuso, 2007: Applying multifractality and the self-organized criticality theory to describe the temporal rainfall regimes in Andalusia (southern Spain). *Hydrol. Processes*, **22**, 295–308, <https://doi.org/10.1002/hyp.6603>.
- Groisman, P. Ya., and Coauthors, 1999: Changes in the probability of heavy precipitation: Important indicators of climatic change. *Climatic Change*, **42**, 243–283, <https://doi.org/10.1023/A:1005432803188>.
- IPCC, 2014: Summary for policymakers. *Climate Change 2014: Impacts, Adaptation, and Vulnerability*, C. B. Field et al., Eds., Cambridge University Press, 1–32.
- Kharin, V. V., F. W. Zwiers, X. Zhang, and M. Wehner, 2013: Changes in temperature and precipitation extremes in the CMIP5 ensemble. *Climatic Change*, **119**, 345–357, <https://doi.org/10.1007/s10584-013-0705-8>.
- Lenderink, G., and E. van Meijgaard, 2008: Increase in hourly precipitation extremes beyond expectations from temperature changes. *Nat. Geosci.*, **1**, 511–514, <https://doi.org/10.1038/ngeo262>.
- Liu, B., M. Xu, M. Henderson, and Y. Qi, 2005: Observed trends of precipitation amount, frequency, and intensity in China, 1960–2000. *J. Geophys. Res.*, **110**, D08103, <https://doi.org/10.1029/2004JD004864>.
- Ma, S., and T. Zhou, 2015: Observed trends in the timing of wet and dry season in China and the associated changes in frequency and duration of daily precipitation. *Int. J. Climatol.*, **35**, 4631–4641, <https://doi.org/10.1002/joc.4312>.
- , —, A. Dai, and Z. Han, 2015: Observed changes in the distributions of daily precipitation frequency and amount over China from 1960 to 2013. *J. Climate*, **28**, 6960–6978, <https://doi.org/10.1175/JCLI-D-15-0011.1>.
- , and Coauthors, 2017: Detectable anthropogenic shift toward heavy precipitation over eastern China. *J. Climate*, **30**, 1381–1396, <https://doi.org/10.1175/JCLI-D-16-0311.1>.
- Martínez-Villalobos, C., and J. D. Neelin, 2018: Shifts in precipitation accumulation extremes during the warm season over the United States. *Geophys. Res. Lett.*, **45**, 8586–8595, <https://doi.org/10.1029/2018GL078465>.
- , and —, 2019: Why do precipitation intensities tend to follow gamma distributions? *J. Atmos. Sci.*, **76**, 3611–3631, <https://doi.org/10.1175/JAS-D-18-0343.1>.
- Muschinski, T., and J. I. Katz, 2013: Trends in hourly rainfall statistics in the United States under a warming climate. *Nat. Climate Change*, **3**, 577–580, <https://doi.org/10.1038/nclimate1828>.
- National Report Committee, 2007: *China’s National Assessment Report on Climate Change* (in Chinese). Science Press, 422 pp.
- Neelin, J. D., S. Sahany, S. N. Stechmann, and D. Bernstein, 2017: Global warming precipitation accumulation increases above the current-climate cutoff scale. *Proc. Natl. Acad. Sci. USA*, **114**, 1258–1263, <https://doi.org/10.1073/pnas.1615333114>.
- Norris, J., G. Chen, and J. D. Neelin, 2019: Changes in frequency of large precipitation accumulations over land in a warming climate from the CESM large ensemble: The roles of moisture, circulation, and duration. *J. Climate*, **32**, 5397–5416, <https://doi.org/10.1175/JCLI-D-18-0600.1>.
- Pendergrass, A. G., 2018: What precipitation is extreme? *Science*, **360**, 1072–1073, <https://doi.org/10.1126/science.aat1871>.
- , and D. L. Hartmann, 2014: Changes in the distribution of rain frequency and intensity in response to global warming. *J. Climate*, **27**, 8372–8383, <https://doi.org/10.1175/JCLI-D-14-00183.1>.
- Peters, O., C. Hertlein, and K. Christensen, 2001: A complexity view of rainfall. *Phys. Rev. Lett.*, **88**, 018701, <https://doi.org/10.1103/PhysRevLett.88.018701>.
- , A. Deluca, A. Corral, J. D. Neelin, and C. E. Holloway, 2010: Universality of rain event size distributions. *J. Stat. Mech.*, **11**, P11030, <https://doi.org/10.1088/1742-5468/2010/11/P11030>.
- Prein, A. F., R. M. Rasmussen, K. Ikeda, C. Liu, M. P. Clark, and G. J. Holland, 2017: The future intensification of hourly precipitation extremes. *Nat. Climate Change*, **7**, 48–52, <https://doi.org/10.1038/nclimate3168>.
- Ren, G., Y. Ren, Y. Zhan, X. Sun, Y. Liu, Y. Chen, and T. Wang, 2015: Spatial and temporal patterns of precipitation variability over mainland China. II: Recent trends (in Chinese). *Adv. Water Sci.*, **26**, 451–465, <https://doi.org/10.14042/j.cnki.32.1309.2015.04.001>.
- , and Coauthors, 2016: Spatial and temporal patterns of precipitation variability over mainland China. III: Causes for recent trends (in Chinese). *Adv. Water Sci.*, **27**, 327–348, <https://doi.org/10.14042/j.cnki.32.1309.2016.03.001>.
- , Y. Ding, and G. Tang, 2017: An overview of mainland China temperature change research. *J. Meteor. Res.*, **31**, 3–16, <https://doi.org/10.1007/s13351-017-6195-2>.
- Ren, Z. H., and Coauthors, 2010: Quality control procedures for hourly precipitation data from automatic weather stations in China (in Chinese). *Meteor. Mon.*, **36**, 123–132.
- Rosenfeld, D., U. Lohmann, G. B. Raga, C. D. O’Dowd, M. Kulmala, S. Fuzzi, A. Reissell, and M. O. Andreae, 2008: Flood or drought: How do aerosols affect precipitation? *Science*, **321**, 1309–1313, <https://doi.org/10.1126/science.1160606>.
- Shi, P., M. Wu, S. Qu, P. Jiang, X. Qiao, X. Chen, M. Zhou, and Z. Zhang, 2015: Spatial distribution and temporal trends in precipitation concentration indices for the Southwest China. *Water Resour. Manage.*, **29**, 3941–3955, <https://doi.org/10.1007/s11269-015-1038-3>.
- Sillmann, J., V. V. Kharin, F. W. Zwiers, X. Zhang, and D. Bronaugh, 2013: Climate extremes indices in the CMIP5 multimodel ensemble: Part 2. Future climate projections. *J. Geophys. Res. Atmos.*, **118**, 2473–2493, <https://doi.org/10.1002/jgrd.50188>.
- Stechmann, S. N., and J. D. Neelin, 2011: A stochastic model for the transition to strong convection. *J. Atmos. Sci.*, **68**, 2955–2970, <https://doi.org/10.1175/JAS-D-11-028.1>.
- , and —, 2014: First-passage-time prototypes for precipitation statistics. *J. Atmos. Sci.*, **71**, 3269–3291, <https://doi.org/10.1175/JAS-D-13-0268.1>.
- Sun, Y., S. Solomon, A. Dai, and R. Portmann, 2007: How often will it rain? *J. Climate*, **20**, 4801–4818, <https://doi.org/10.1175/JCLI4263.1>.
- Trenberth, K. E., 2011: Changes in precipitation with climate change. *Climate Res.*, **47**, 123–138, <https://doi.org/10.3354/cr00953>.

- Wang, Y., and L. Zhou, 2005: Observed trends in extreme precipitation events in China during 1961–2001 and the associated changes in large-scale circulation. *Geophys. Res. Lett.*, **32**, L09707, <https://doi.org/10.1029/2005GL023769>.
- Wasko, C., and R. Nathan, 2019: The local dependency of precipitation on historical changes in temperature. *Climatic Change*, **156**, 105–120, <https://doi.org/10.1007/s10584-019-02523-5>.
- Westra, S., L. V. Alexander, and F. W. Zwiers, 2013: Global increasing trends in annual maximum daily precipitation. *J. Climate*, **26**, 3904–3918, <https://doi.org/10.1175/JCLI-D-12-00502.1>.
- Xu, X., Y. Du, J. Tang, and Y. Wang, 2011: Variations of temperature and precipitation extremes in recent two decades over China. *Atmos. Res.*, **101**, 143–154, <https://doi.org/10.1016/j.atmosres.2011.02.003>.
- Xu, Y., X. Gao, F. Giorgi, B. Zhou, Y. Shi, J. Wu, and Y. Zhang, 2018: Projected changes in temperature and precipitation extremes over China as measured by 50-yr return values and periods based on a CMIP5 ensemble. *Adv. Atmos. Sci.*, **35**, 376–388, <https://doi.org/10.1007/s00376-017-6269-1>.
- Yang, P., J. Xia, Y. Zhang, and S. Hong, 2017: Temporal and spatial variations of precipitation in Northwest China during 1960–2013. *Atmos. Res.*, **183**, 283–295, <https://doi.org/10.1016/j.atmosres.2016.09.014>.
- Yang, Q., Z. Ma, X. Fan, Z. Yang, Z. Xu, and P. Wu, 2017: Decadal modulation of precipitation patterns over eastern China by sea surface temperature anomalies. *J. Climate*, **30**, 7017–7033, <https://doi.org/10.1175/JCLI-D-16-0793.1>.
- You, Q., and Coauthors, 2011: Changes in daily climate extremes in China and their connection to the large scale atmospheric circulation during 1961–2003. *Climate Dyn.*, **36**, 2399–2417, <https://doi.org/10.1007/s00382-009-0735-0>.
- Zhai, P. M., X. Zhang, H. Wan, and X. Pan, 2005: Trends in total precipitation and frequency of daily precipitation extremes over China. *J. Climate*, **18**, 1096–1108, <https://doi.org/10.1175/JCLI-3318.1>.
- Zhang, R.-H., 2015: Natural and human-induced changes in summer climate over the east Asian monsoon region in the last half century: A review. *Adv. Climate Change Res.*, **6**, 131–140, <https://doi.org/10.1016/j.accre.2015.09.009>.
- Zhang, W., and T. Zhou, 2019: Significant increases in extreme precipitation and the associations with global warming over the global land monsoon regions. *J. Climate*, **32**, 8465–8488, <https://doi.org/10.1175/JCLI-D-18-0662.1>.
- Zheng, Z. F., and G. Ren, 2017: Effects of gauge under-catch on precipitation observation and long-term trend estimates in Beijing area (in Chinese). *Adv. Water Sci.*, **28**, 662–670, <https://doi.org/10.14042/j.cnki.32.1309.2017.05.003>.
- Zhou, B., Y. Xu, J. Wu, S. Dong, and Y. Shi, 2016: Changes in temperature and precipitation extreme indices over China: Analysis of a high-resolution grid dataset. *Int. J. Climatol.*, **36**, 1051–1066, <https://doi.org/10.1002/joc.4400>.